Korea-Australia Rheology Journal
Vol. 22, No. 1, March 2010 pp. 31-41

Capillary breakup extensional rheometry of a wormlike micellar solution

Nahn Ju Kim[1,2], Christopher J. Pipe[2], Kyung Hyun Ahn[1], Seung Jong Lee[1] and Gareth H. McKinley[2,*]
[1]*School of Chemical and Biological Engineering, Seoul National University, Seoul 151-744, Republic of Korea*
[2]*Hatsopoulos Microfluids Laboratory, Department of Mechanical Engineering, Massachusetts Institute of Technology, Cambridge, MA 02139, USA*

(Received September 5, 2009)

Abstract

The behaviour of a cetylpyridinium chloride/sodium salicylate wormlike micellar system undergoing capillary breakup is investigated experimentally. The transient elongational flow induced in a thinning thread is used to study the apparent viscosity and effective relaxation time of the micellar network in extension. The sensitivity of the material response to initial conditions and deformation history is explored by varying the endplate diameter of the capillary breakup rheometer and the initial step strain imposed on the sample. Local regimes in which the extensional viscosity shows constant (Newtonian), weak extensional thinning and strong extensional thickening are observed depending on the accumulated strain and strain rate. For this concentrated micellar network, the relaxation time determined in extension was found to be independent of the initial configuration and in close agreement with the value measured in shear flow.

Keywords **:** wormlike micellar solution, capillary breakup extensional rheometry, complex transient response, extensional relaxation time

1. Introduction

Above a critical concentration, amphiphilic surfactant molecules in solution can spontaneously assemble to form wormlike micelles. The weak ionic bonds between the surfactant molecules allow the micellar chains to break and recombine reversibly and continuously, giving rise to the name 'living polymers'. These semi-dilute surfactant solutions are commonly found in personal care products as well as having important applications in the oilfield industry. While the shear rheology of these complex fluids has been the focus of many experimental, numerical and theoretical studies, the response in extensional flows remains relatively unexplored.

There are many different wormlike micellar systems, each having a unique thermodynamic and rheological signature depending on the particular surfactant, counterion, solvent and the relative concentrations of each species (Rehage and Hoffman, 1991; Larson, 1998). In the following we shall limit our discussion to the behaviour common to semi-dilute shear-banding systems of wormlike micelles far from any phase transitions. For linear shearing deformations with characteristic times much greater than the timescale of micellar breakage and recombination, stress relaxation in the micellar network is conducted by reptation and the breaking of micellar strands. The macroscopic material response can be well approximated by a single mode Maxwell liquid with shear viscosity η and relaxation time λ (Rehage and Hoffmann, 1991). As the timescale of the applied deformation approaches the timescale of micellar breakage and recombination, breathing or Rouse modes of stress relaxation become important and the measured behaviour deviates from the Maxwell model (Turner and Cates, 1991). The initial transient response can also be well represented using a convected Maxwell model for linear deformations with characteristic timescales $\dot{\gamma}<1/\lambda$ where λ is the bulk relaxation time of the fluid (Pipe *et al.*, Submitted). At faster deformation rates, large non-linear stress transients can be observed on timescales $t\sim\lambda$ (Fischer and Rehage, 1997). The steady-state viscous response to an imposed shear rate is characterized by a Newtonian response at low shear rates and the appearance of a plateau in the shear stress at $\dot{\gamma}\sim 1/\lambda$ which is associated with the onset of shear-banded flow (Britton and Callaghan, 1997). The development of shear-banded flow can lead to transients in the stress response lasting many hundreds of elastic relaxation times before steady-state flow is attained (Grand *et al.*, 1997; Pipe *et al.*, Submitted). At high shear rates $\dot{\gamma}\sim 100\ s^{-1}$ the shear stress plateau is superseded by a region where the shear stress increases with shear rate (Nghe *et al.*, 2008; Pipe *et al.*, 2008). In summary, for shearing flows the response is well described by a simple convected Maxwell model for small deformation rates.

*Corresponding author: gareth@mit.edu

Although the behaviour is highly non-linear for shear rates $\dot{\gamma} > 1/\lambda$, such flows can be calculated using more sophisticated microstructural models (Dhont and Briels, 2008; Vasquez *et al.*, 2007).

Industrial applications involving wormlike micellar solutions, however, often involve complex deformations with both shear and extensional components. Investigations using a range of wormlike micellar liquids by Belmonte and coworkers (Akers and Belmonte, 2006; Jayaraman and Belmonte, 2003; Smolka and Belmonte, 2003; Sostarecz and Belmonte, 2004) into flows containing significant shear and extensional components have highlighted the importance of understanding the response to extensional deformations.

Early attempts to characterize the extensional behaviour of micellar liquids were carried out using opposed nozzles experiments by Prud'homme and Warr (1994) and Walker *et al.* (1996) who studied tetradecyltrimethylammonium bromide/sodium salicylate (TTABr/NaSal) and cetylpyridinium chloride/sodium salicylate (CPyCl/NaSal) wormlike micellar systems, respectively. Three distinct responses to uniaxial extensional deformations were noted: a constant extensional viscosity at low extension rates, followed by a regime of extension-thickening in which the measured tensile stress difference reaches an order of magnitude greater than the low extension rate response. Beyond a critical extension rate the extensional viscosity then decreases substantially with strain rate. At low Deborah number $De = \lambda\dot{\varepsilon} < 0.5$, where $\dot{\varepsilon}$ is the extension rate, the extensional viscosity was found to be the same order of magnitude as, but greater than, the predicted value of three times the zero shear viscosity (Prud'homme and Warr, 1994; Walker *et al.*, 1996). However, this discrepancy from the expected Newtonian response was attributed to the measurement technique. Walker *et al.* (1996) found the onset in increasing extensional viscosity to occur at $De \approx 0.7$, consistent with the behaviour of a Maxwellian viscoelastic liquid. For $De > 5$ an extensional viscosity decreasing with extension rate was recorded and extensional viscosities approached the low extension rate value at $De \approx 100$. The extension-thinning behaviour was attributed to breaking of the micellar chains due to strong extensional deformations; this hypothesis was reinforced by birefringence measurements in the opposed nozzles configuration by Chen and Warr (1997) in which a decrease in the radius of gyration of wormlike TTABr/NaSal micelles was observed to coincide with the decrease in extensional viscosity. Opposed nozzles experiments using branched wormlike micellar fluids (Fischer *et al.*, 1997) indicated that the increase in extensional viscosity occurred at deformation rates of the same order of magnitude as the value for which shear-thinning behaviour was seen in shear flow. The onset of extensional thickening followed by subsequent thinning in micellar networks is similar to the response of entangled polymer melts.

More recently, transient extensional rheology results from filament stretching experiments by Rothstein and coworkers (Bhardwaj *et al.*, 2007a; Bhardwaj *et al.*, 2007b; Rothstein, 2003) have confirmed a transient extensional thickening (also referred to as strain-hardening) response for cetyltrimethylammonium bromide/sodium salicylate (CTAB/NaSal) and CPyCl/NaSal solutions. An increasing extensional viscosity with accumulated extensional strain was noted as well as filament rupture and decreasing values of the extensional viscosity for increasing extension rates. This latter observation was suggested as symptomatic of the fall in extensional viscosity at large Deborah numbers previously observed in opposed nozzles experiments. Microstructural constitutive models that capture the reptation and rupture mechanisms present in the transient micellar network predict both of these observations (Cromer *et al.*, 2009).

Capillary breakup experiments with micellar solutions (Bhardwaj *et al.*, 2007a; Bhardwaj *et al.*, 2007b; Yesilata *et al.*, 2006) have been used to investigate the characteristic relaxation times in extensional flows. The relaxation times of CPyCl/NaSal and CTAB/NaSal solutions measured from capillary breakup experiments were in good agreement with those found from small amplitude oscillatory shear measurements (Bhardwaj *et al.*, 2007a; Bhardwaj *et al.*, 2007b). However, measurements using erucyl bis(2-hydroxyethyl) methyl ammonium chloride (EHAC) by Yesilata *et al.* (2006) found the relaxation time in capillary-thinning experiments to be approximately a third of the relaxation time measured in shear flow. The source of the discrepancy between the viscoelastic relaxation times found in these two studies is not clear, and as discussed by McKinley (2005) the appropriate analysis for entangled solutions in capillary breakup extensional rheometer (CaBER) experiments is not yet well understood. Numerical and experimental investigations of concentrated entangled polymer solutions undergoing filament stretching have shown that the measured extensional response can be a sensitive function of experimental geometry, fluid microstructure and strain history (Bhattacharjee *et al.*, 2002; Liang and Mackley, 1994; Yao *et al.*, 2000) and it is not surprising that such highly non-linear systems are sensitive to initial conditions. In a recent report by Rothstein and coworkers (Miller *et al.*, 2009), the extensional relaxation time of CPyCl/NaSal system was found to decrease rapidly as the stretching speed and stretching distance in CaBER measurements were increased, and finally reached an asymptotic plateau value at around 50% of the value of the shear relaxation time.

In order to better understand the apparent extensional properties of semi-dilute wormlike micellar solutions in capillary-thinning measurements we undertake a systematic study of the role of geometric configuration and strain history on the capillary breakup behaviour of a CPyCl/NaSal system after a step extensional strain. In contrast to

the work by Miller *et al.* (2009), which covers a wide range of stretching parameter space using a geometry of fixed size, in the present study the size of geometry as well as the stretching distance is varied. In Section 2 we detail the test fluid and the experimental protocol; in Section 3 we present measurements of the extensional viscosity and the relaxation time as a function of endplate diameter and the initial step strain; finally in Section 4 we conclude our findings on how CaBER experiments can be used to investigate the behaviour of highly non-linear fluids.

2. Experimental test

2.1. Test Fluid

The wormlike micellar solution used in this study is cetylpyridinium chloride (100 mM)/sodium salicylate (50 mM) solution in 100 mM NaCl brine (CPyCl/NaSal solution in brine), and is similar to the fluids used in a number of previous studies (Berret *et al.*, 1993; Berret *et al.*, 1994; Berret *et al.*, 1997; Bhardwaj *et al.*, 2007a; Bhardwaj *et al.*, 2007b; Britton *et al.*, 1999; Davies *et al.*, 2010; Hu and Lips, 2005). This system is well above the critical micelle concentration (Lee *et al.*, 2005) and located in the semi-dilute concentration regime (Berret *et al.*, 1997) far from any concentration or shear-induced phase transitions. Cetylpyridinium chloride (MP Biomedical) was dissolved in distilled water with a magnetic stirrer and sodium salicylate (Sigma Aldrich) was added. Sodium chloride (Mallinckrodt Chemicals) was added last. After an hour of mixing, the mixture was set to rest overnight to allow bubbles to rise before use.

The shear rheology of the wormlike micellar solution was measured using an ARES rheometer (TA Instruments). Steady shear tests were performed using a 50 mm/0.0402 rad cone-and-plate geometry at 22°C. Below shear rates of 1 s^{-1}, the fluid exhibits a constant viscosity. At higher rates, the fluid shows strong shear-thinning behaviour and a plateau in the shear stress at $\tau = 21$ Pa is observed (Fig. 1 (a)). By fitting an empirical Carreau-Yasuda model to the rate-dependent viscosity η as a function of the shear rate $\dot{\gamma}$:

$$\eta = \eta_0[1+(\lambda\dot{\gamma})^a]^{(n-1)/a} \quad (1)$$

we determine the zero shear viscosity $\eta_0 = 17$ Pa·s, the relaxation time $\lambda = 0.88$ s, the power-law exponent $n = 0.0071$ and the dimensionless fitting parameter $a = 2.2$.

Small amplitude oscillatory shear tests were performed using the same geometry at temperatures T=20, 22, 30 and 40°C. To reduce the effects of sample loading and stress history the fluid sample was pre-sheared at 1 s^{-1} for 2 minutes and then left to rest for 2 minutes before starting the measurements. The elastic and loss moduli for each temperature collapsed by time-temperature superposition are shown in Fig. 1 (b), where 22°C is chosen as the reference temperature. The excellent superposition indicates a good level of reproducibility for measurements of the shear properties of the system across the temperature range investigated. Classic Maxwellian behaviour is observed at low frequencies and fitting a single mode Maxwell model to the data for $10^{-2} < \omega < 10^{2}$ rad/s gives an elastic plateau modulus $G_N^0 = 24.0$ Pa and a Maxwell relaxation time $\lambda_M = 0.64$ s at T=22°C. At high frequencies $\omega > 10^2$ rad/s the response of the wormlike micelles is dominated by Rouse-like motion and the material behaviour departs from a single mode Maxwell model (Turner and Cates, 1991). Further details of the shear rheology of this system and the ability of microstructural models to describe the measurements are given by Pipe *et al.* (Submitted).

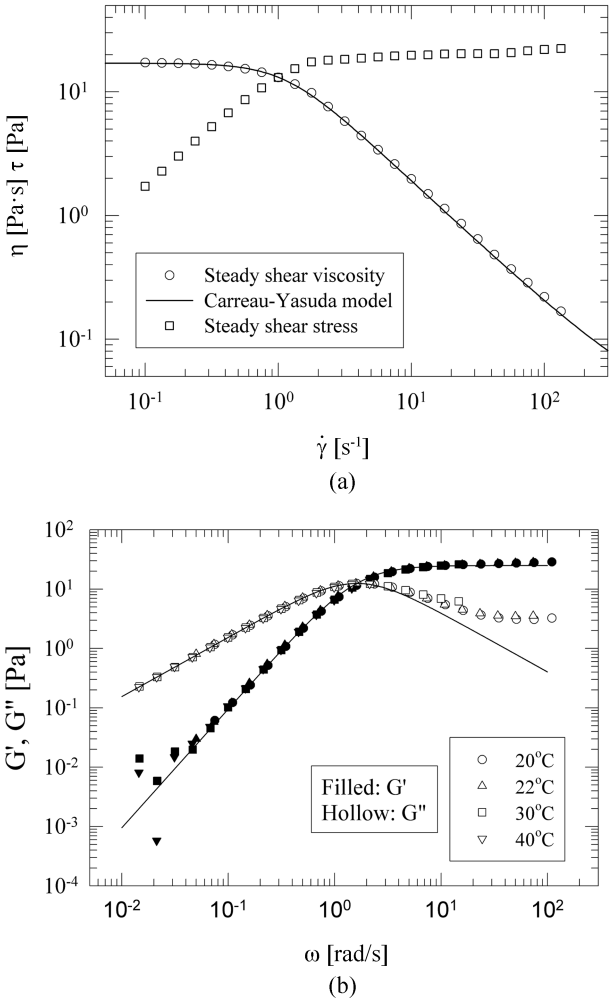

Fig. 1. (a) Steady shear rate viscosity η and shear stress τ measured as a function of shear rate $\dot{\gamma}$ and (b) storage modulus G' and loss modulus G'' measured in small amplitude oscillatory shear experiments for the CPyCl/NaSal micellar system. Measurements are shifted to a reference temperature of 22°C.

2.2. Capillary breakup extensional rheometry measurements

The aim of the CaBER technique is to impose a predominantly-uniaxial extensional step deformation on a liquid

sample in order to extract information on its transient extensional properties (McKinley, 2005). The initial liquid bridge is formed by loading a fluid sample between two endplates of diameter D_0 separated by initial height h_0. In order to keep this initial configuration stable and close to cylindrical, the initial distance between endplates h_0 is kept smaller than capillary length $l_{cap} = \sqrt{\sigma/\rho g}$ (Rodd *et al.*, 2005). With the surface tension measured to be $\sigma = 30 \pm 0.6$ mN/m at 24°C using a ring tensiometer, and the density $\rho = 1045$ kg/m^3 (Miller and Rothstein, 2007), the capillary length of the CPyCl/NaSal solution is $l_{cap} = 1.7$ mm. Thus the initial displacement was held constant at $h_0 = 1.0$ mm for all measurements in this study to give an approximately uniform cylindrical sample before stretching.

At time $t = -50$ ms, the upper endplate is displaced upward following an exponential profile $h(t) = h_0 e^{+\dot{\varepsilon}_0 t}$ and achieves the final height h_f at $t = 0$ s. Final heights in the range $3.91 < h_f < 6.37$ mm were used, giving stretching rates up to $\dot{\varepsilon}_0 = 37.0$ s^{-1} during the initial stretch: if h_f was too small, the filament did not breakup but remained in a necked but stable liquid bridge configuration; on the other hand, if h_f was too large, the fluid filament ruptured through mechanisms different to capillary-thinning and breakup (Bhardwaj *et al.*, 2007a; Cromer *et al.*, 2009; McKinley, 2005) and this was also avoided. Since the ratio of surface area to volume is large for a liquid sample undergoing capillary breakup, evaporation of the sample may be critical. To prevent significant drying of the sample, configurations resulting in capillary breakup times t_c in the range $5 < t_c < 12$ s were used. Hereafter, final heights are expressed in terms of the final aspect ratio of the sample $\Lambda_f \equiv h_f/D_0$.

The evolution in the filament diameter at the midplane of the fluid column ($h = h_f/2$) was monitored using a laser micrometer (Z4LA-1030, Omron Electronics) with an effective accuracy of 20 μm at a sampling frequency of 50 Hz. The evolution of the liquid bridge breakup process was also recorded by video camera (TM-200, PULNiX).

For a cylindrical filament, the axial force balance gives

$$\Delta\tau(t) = 3\eta\dot{\varepsilon} + (\tau_{p,zz} - \tau_{p,rr}) = \frac{2\sigma}{D(t)} \tag{2}$$

where $\Delta\tau(t)$ is the capillary pressure exerted on the fluid filament during the necking process. Further details of this force balance can be found in McKinley (2005). Following the standard analysis of capillary breakup experiments (Anna and McKinley, 2001; Entov and Hinch, 1997), we define the instantaneous Hencky strain ε and strain rate $\dot{\varepsilon}$ in the fluid filament as:

$$\varepsilon(t) = 2\ln\left(\frac{D_0}{D(t)}\right) \tag{3}$$

$$\dot{\varepsilon}(t) = \frac{d\varepsilon(t)}{dt} = -\frac{2}{D(t)}\frac{dD(t)}{dt} \tag{4}$$

Using the force balance in Eq.(2), the *apparent* extensional viscosity of the fluid at any instant can also be determined from the diameter measurement:

$$\eta_E \equiv \frac{\Delta\tau(t)}{\dot{\varepsilon}(t)} \approx -\frac{\sigma}{dD(t)/dt} \tag{5}$$

It is important to note that such a definition is an 'apparent' or 'effective' measure of the extensional viscosity and is a path-dependent quantity that depends on the deformation history (Petrie, 2006). If the flow in the thinning bridge can be modeled, then this history-dependence can be understood.

For a purely viscous liquid, the filament diameter decreases linearly with time. Papageorgiou (1995a, 1995b) showed that, for an inertialess Newtonian fluid thread thinning under capillarity, the thread shape is self-similar and the midpoint diameter varies as:

$$\frac{D(t)}{D_0} = 0.0709\frac{2\sigma}{\eta D_0}(t_c - t) \tag{6}$$

The numerical prefactor in Eq. (6) arises from the form of the similarity solution. Substitution into Eq. (5) shows that the resulting definition of apparent viscosity does not give the expected Trouton result for a Newtonian fluid $\eta_E = 3\eta$. A more complete analysis of the extensional flow in the neck then suggests that a better definition of the apparent extensional viscosity incorporating the non-zero tensile force $F_z(t) = 2X\pi\sigma R(t)$ in the fluid column is needed. This gives

$$\eta_E = \frac{\Delta\tau(t)}{\dot{\varepsilon}(t)} = -(2X-1)\frac{\sigma}{dD/dt} \tag{7}$$

where X depends on the local shape $R(z,t)$ of the filament (where z denotes the axial coordinate along the filament), which itself depends on the balance of appropriate forces in the similarity solution (McKinley and Tripathi, 2000). For the self-similar Papageorgiou solution $X = 0.7127$ (Papageorgiou, 1995b).

Varying the initial aspect ratio of a sample or the diameter of the endplates in a CaBER experiment affects the shape of the filament formed after the step deformation is applied. This in turn affects the subsequent rate of evolution in the filament radius as it collapses towards the self-similar solution, and thus, through Eqs. (6) and (7) affects the apparent extensional viscosity.

The situation can be even more complicated for a complex fluid with a strain- and rate-dependent extensional viscosity. For a model viscoelastic fluid (such as a dilute polymer solution) the elastic stress dominates at large strain. As a result, the fluid column is closer to purely cylindrical and the diameter decreases exponentially as a function of time (Entov and Hinch, 1997; McKinley, 2005). It thus follows that at large times (strains) the strain rate in the thinning fluid column is dependent solely on the

longest extensional relaxation time λ_E:

$$\frac{D(t)}{D_0} = \left(\frac{GD_0}{4\sigma}\right)^{1/3} \exp[-t/3\lambda_E] \quad \Leftrightarrow$$

$$\dot{\varepsilon}(t) = -\frac{2}{D(t)}\frac{dD(t)}{dt} = \frac{2}{3\lambda_E} \qquad (8a, b)$$

As a result, the dimensionless rate of stretching (which may be referred to as a Weissenberg number or Deborah number) $De = \lambda_E \dot{\varepsilon}$ in the thinning filament tends to a constant value $De = 2/3$ in the elastic limit (Entov and Hinch, 1997).

We also can define a different ratio of intrinsic times (which is thus also truly a Deborah number) using the material relaxation time and the Rayleigh timescale for inertiocapillary breakup. We denote this intrinsic Deborah number as:

$$De_{int} = \frac{\lambda}{t_R} = \frac{\lambda}{\sqrt{\rho R_0^3/\sigma}} \qquad (9)$$

This dimensionless quantity is referred to as an 'intrinsic' quantity because the necking process is not controlled externally but rather the strain rate is self-selected by the fluid (Rodd *et al.*, 2005). Once the material and the dimensions of the test geometry are chosen, this dimensionless group is constant. To explore the role of the intrinsic Deborah number, a range of endplate diameters were adopted. Apart from the original stainless steel endplates with $D_0 = 6.0$ mm, smaller endplates with $D_0 = 4.76$ mm and $D_0 = 3.18$ mm were manufactured from plastic rods (Delrin®, Quadrant Engineering Plastic). Fresh adhesive-backed sandpaper disks (prepared with a circular punch) were attached to the endplates before each experiment to prevent the fluid detaching from the somewhat hydrophobic plastic endplates during the initial stretch. The experiments were performed at ambient temperature: 22 ± 0.5°C for the tests using steel endplates and 18 ± 0.5°C for the tests using plastic ones. For the test fluids used in the present study this gave intrinsic Deborah numbers of 60, 32, and 23 for the 3.18 mm, 4.76 mm and 6.0 mm endplates respectively.

In contrast to previous CaBER experiments with wormlike micelles (Bhardwaj *et al.*, 2007a; Bhardwaj *et al.*, 2007b; Miller *et al.*, 2009; Yesilata *et al.*, 2006), we choose not to fit a viscoelastic fluid model to the data to calculate the response in extension. While this allows the material behaviour to be determined independently of any *a priori* assumptions, the experimental noise can consequently become large as the filament diameter approaches the resolution of the laser micrometer in the calculated strain rate and extensional viscosity because they are local point-wise calculations of the needed time derivative $dD(t)/dt$. Since the noise is at a higher frequency than the slow changes in the filament diameter, a low pass filter was generated using MATLAB® software and applied to the measured diameter.

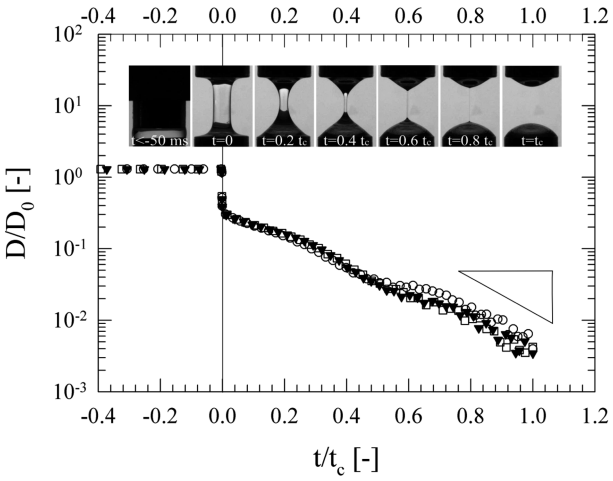

Fig. 2. Stretching profile and matched video clip of CPyCl/NaSal solution with $D_0 = 6$ mm endplates, final distance between endplates $h_f = 6.29$ mm, and resulting final aspect ratio $\Lambda_f = h_f/D_0 = 1.05$. The rate of thinning is indicated at later times during the viscoelastic capillary-thinning regime. Breakup times were 13.1, 11.4 and 11.0 s, and the evaluated extensional relaxation times were $\lambda_E = 0.97$, 0.68 and 0.78 s indicated by the symbols ○, ▼, and □ respectively.

The time derivative of the low-pass filtered diameter was calculated using a second-order center difference method. Furthermore, for visual clarity only one of every ten data points is shown in the figures.

3. Results and discussion

3.1. Filament profile

We start by presenting the evolution in the non-dimensional midpoint diameter D/D_0 for the CPyCl/NaSal thread during a CaBER experiment in Fig. 2. These data are for 6 mm endplates and a final stretching aspect ratio $\Lambda = 1.05$. The evolution of the minimum diameter of the liquid bridge is shown as a function of the non-dimensional time t/t_c where the time $t/t_c = 0$ corresponds to the end of the applied step extensional strain. Three data sets for the same experimental conditions are shown to indicate the level of repeatability of the capillary-thinning process and the breakup times for the three experiments are $t_c = 13.1$, 11.4 and 11.0 s. This variation in breakup time is due to small differences in the initial experimental conditions and the loading of the sample, however, the experimental reproducibility between runs is sufficient to evaluate the general behaviour of the micellar solution during the transient extensional flow associated with capillary-thinning. Also shown in Fig. 2 are images of the thinning liquid bridge during the experiment. For $t/t_c \leq 0.4$ the liquid bridge shows an hourglass profile characteristic of Newtonian and shear-thinning elastic liquids (Yao *et al.*, 2000) while at longer times $t/t_c \geq 0.6$,

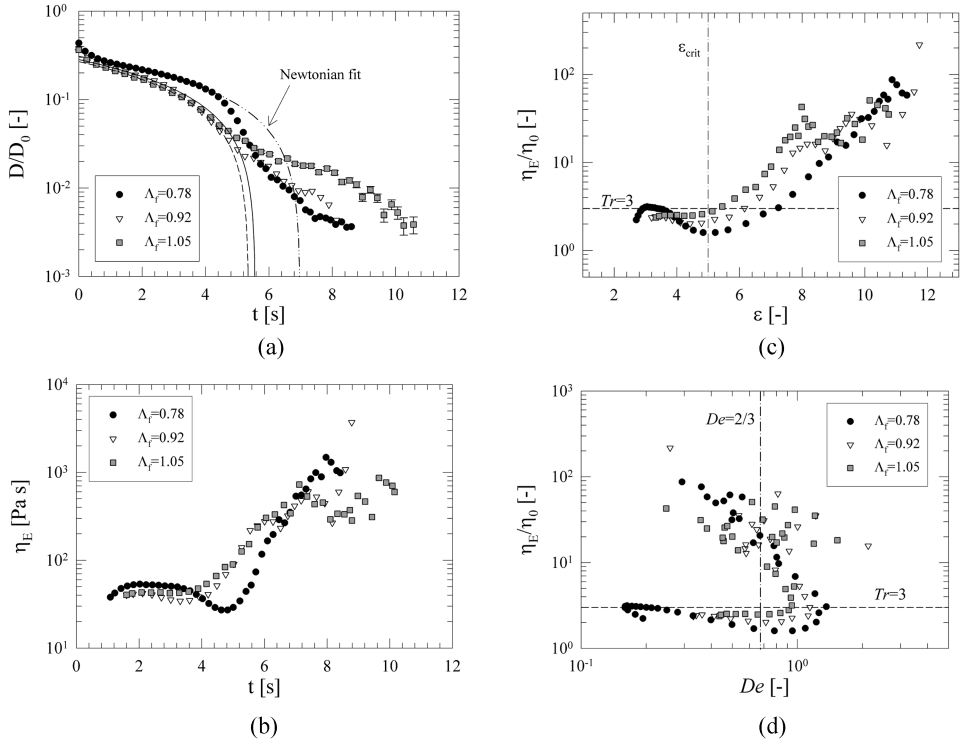

Fig. 3. Capillary-thinning profiles of CPyCl/NaSal solution with endplate diameter D_0=6 mm and for the final aspect ratios Λ_f indicated by the legends: (a) instantaneous midpoint diameter D/D_0 of the filament as a function of the elapsed time t, (b) apparent extensional viscosity η_E as a function of time t, (c) Trouton ratio η_E/η_0 as a function of accumulated strain ε at the filament midpoint, and (d) Trouton ratio as a function of the instantaneous non-dimensional filament strain rate $De=\lambda_E\,\dot{\varepsilon}(t)$. The resolution of the measured diameter is indicated by the error bars in (a).

a thin cylindrical liquid column joining the upper and lower reservoirs at the endplates is seen, similar to profiles for highly elastic polymer solutions (McKinley, 2005). The dominant relaxation time in extension was obtained by fitting Eqs. (8a, b) to the viscoelastic strain-hardening regime at $t/t_c \geq 0.6$ where an approximately mono-exponential decay in filament diameter was observed. Extensional relaxation times of 0.97, 0.68 and 0.78 s were measured giving a mean value of 0.81 ± 0.15 s (the error is calculated from the standard deviation) which is slightly larger than, but of the same order as, the value λ = 0.64 s determined from small amplitude shear flow.

3.2. Varying the applied step strain, Λ_f

In Fig. 3 measurements employing different final heights for the same fixed 6 mm endplates are presented in order to explore the effect of the initial step strain amplitude imposed on the CPyCl/NaSal solution at the beginning of the filament-thinning process. Representative plots for each test condition are shown for each final height and the strain, strain rate and extensional viscosity are calculated from the diameter profile using Eqs. (3)-(5).

The final aspect ratios of the three different experiments in Fig. 3 correspond to Λ_f = 0.78, 0.92, and 1.05, and it is clear that different initial stretch amplitudes lead to different material histories. To give an indication of the result expected for a viscous Newtonian liquid, lines showing constant viscosity fits to the data are shown and these indicate an apparent Newtonian viscosity of 16.1, 14.0 and 14.2 Pa·s respectively for the filament-thinning dynamics at short times (t/t_c<0.5). These are in excellent agreement with the measured zero shear viscosity of η_0 = 17 Pa·s for T = 22°C. At intermediate times, two differing behaviours are observed depending on the initial strain: for the smallest strain Λ_f = 0.78 the midpoint diameter decreases more quickly than the Newtonian fluid indicating a rate-thinning viscosity, while for the largest strain Λ_f = 1.05 the filament quickly enters a strain-hardening regime in which the diameter decreases more slowly than expected for the Newtonian fluid and shows an approximately mono-exponential decay indicative of significant viscoelastic tensile stresses in the thinning thread. The intermediate step strain experiment Λ_f = 0.92 demonstrates a small amount of thinning before the onset of strain-hardening. At long times, strain-hardening is observed for all aspect ratios and relaxation times of 0.45 ± 0.06 s, 0.64 ± 0.07 s and 0.81 ± 0.15 s were calculated for Λ_f = 0.78, 0.92 and 1.05 respectively. This demonstrates a clear increase in the measured vis-

coelastic relaxation time λ_E with increasing initial strain amplitude. This will be discussed in greater depth in Section 3.3.

The above observations based on inspection of the filament midpoint diameter can alternatively be viewed in terms of the extensional viscosity calculated as a function of time from Eq. (5). Fig. 3(b) allows us to compare the evolution of the filament diameter in relation to the extensional viscosity. As expected, when the radius decreases more quickly than is observed for a Newtonian liquid, an extensional thinning viscosity is calculated; when the radius decreases more slowly than a Newtonian liquid an extensional thickening viscosity is measured. We shall discuss the features of the measured extensional viscosity in greater detail below.

In Fig. 3(c) the non-dimensional extensional viscosity η_E / η_0 (commonly referred to as the Trouton ratio Tr) is shown as a function of the Hencky strain accumulated at the midpoint of the filament. For a Newtonian liquid $Tr=3$ independent of the accumulated strain, whereas for viscoelastic fluids in step extensional strain experiments at large strains, an extensional viscosity monotonically increasing with accumulated strain resulting in values of $Tr \sim 100$ are commonly observed (Anna and McKinley, 2001; Kojic *et al.*, 2006). The results show both these limits for the CPyCl/NaSal solution with a Trouton ratio $Tr=3$ at low strains ($\varepsilon \sim 3$) when viscous forces dominate, and strain-hardening leading to a Trouton ratio $Tr \sim 100$ at large strains ($\varepsilon \sim 10$). At intermediate strains ($\varepsilon \sim 4$) some transient extensional thinning is observed in the viscosity leading to Trouton ratios $Tr < 3$. This is most marked for the smallest value of final aspect ratio (Λ_f=0.78) and is similar to experimental and numerical results reported by Bhattacharjee *et al.* (2002). In this earlier work, an extensionally-thinning viscosity is found for capillary-thinning flows of entangled polymer solutions using a filament stretching apparatus. In those experiments the reduction in viscosity was attributed to alignment of the chains in the entangled polymer network before the onset of chain stretching. A reduction in the apparent extensional viscosity has not been observed in tests with either opposed nozzles experiments – which generate an Eulerian steady flow at a fixed apparent extension rate (Prud'homme and Warr, 1994; Walker *et al.*, 1996) – or in controlled rate filament stretching experiments which impose a constant extension rate at the filament midpoint (Bhardwaj *et al.*, 2007a; Rothstein, 2003) or previous CaBER measurements where the kinematics are self-selected by the thinning filament (Bhardwaj *et al.*, 2007a; Yesilata *et al.*, 2006).

While it is possible that an apparent reduction in η_E was not resolved in previous steady-state experiments with micelles due to flow rearrangement in the opposed nozzles experiments or due to a lack of resolution at low strains in filament stretching experiments or due to the different geometrical configuration and analysis techniques employed previously in CaBER tests, we argue that the apparent extensional thinning response seen here is caused by viscous rearrangement of the liquid bridge rather than being characteristic of the viscous response in extension. As shown in Fig. 2, the liquid bridge does not attain the well-defined and predominantly-cylindrical configuration anticipated for a viscoelastic filament until the strain-hardening regime. Therefore rearrangement/redistribution of the upper and lower fluid reservoirs may significantly affect the measured evolution of the midpoint diameter. The filament is not long and slender as assumed in the original analysis, and the fluid dynamics of free-surface filament-thinning are coupled with the rheometric changes in the strain-dependent material rheology. As the final aspect ratio is increased to 1.05, the extensional thinning behaviour disappears. Since the final aspect ratios in other studies using a similar system were comparably bigger: $\Lambda_f = 1.8$ in Bhardwaj *et al.* (2007a), and $1.5 < \Lambda_f < 7.5$ in Miller *et al.* (2009), it can be anticipated that extensional thinning would not be observed in these measurements.

The onset of strain-hardening is observed at $\varepsilon_{crit} = 5$, shown by the dashed vertical line in Fig. 3 (c), for all initial step strain amplitudes tested. Whether this critical strain value is related to an underlying material property or is rather a feature of the experimental setup is not certain. While observed for all experiments conducted in the present study, previous CaBER experiments using a similar system do not show an onset of strain-hardening from a low strain constant viscosity region (Bhardwaj *et al.*, 2007a; Miller *et al.*, 2009): this could, however, be due to the model fit applied to the data in the cited work not providing a sufficiently faithful description of the thinning filament behaviour at short times.

In the strain-hardening regime the extensional viscosity depends on the initial step strain: as the magnitude of the initial step strain is increased, so a greater apparent extensional viscosity is observed at the filament midpoint for a given accumulated strain. This observation underlines the importance of the strain history on the capillary-thinning dynamics and the measured extensional viscosity. At large accumulated strains, the filament diameter decreases below the resolution of the laser micrometer and the final value of the Trouton ratio ($Tr \sim 100$) is in good agreement with previous work (Bhardwaj *et al.*, 2007a; Yesilata *et al.*, 2006). However, Miller *et al.* (2009) reported that when the final stretch was increased to values more than $\Lambda_f = 1.5$, the final value of the Trouton ratio was decreased to $Tr \sim 10$.

We next turn to an examination of the extensional viscosity as a function of the instantaneous extension rate and show the Trouton ratio as a function of the non-dimensional strain rate ($De = \lambda_E \dot{\varepsilon}$) in Fig. 3(d). Similar behaviour is observed for all starting configurations tested: initially the Trouton ratio $Tr \approx 3$ within experimental error and the

extension rate increases monotonically as we would expect for a viscous liquid (see Eqs. (4) and (6)). A mild thinning in the apparent extensional viscosity is observed as the non-dimensional strain rate approaches a maximum value $De \approx 1$. As viscoelasticity becomes increasingly important, the apparent extensional viscosity increases and the extension rate falls approaching a long-time asymptote of $De \approx 2/3$ as predicted by a one dimensional analysis of the thinning filament (Anna and McKinley, 2001). Measurement error is large due to the small diameter of the sample at these long times and is further amplified by the numerical differentiation used to calculate the strain rate.

The flow curves observed in these transient experiments appear very different to those reported by Walker *et al.* (1996) where a constant extensional viscosity is measured at low extension rates ($De < 0.7$) with an increase in the extensional viscosity at extension rates $De > 0.7$, followed by a decrease at $De > 5$. However, it must be borne in mind that, contrary to the opposed nozzles device where the apparent extension rate is steady-state experiments (Walker *et al.*, 1996), the extension rate experienced during filament-thinning experiments is self-selected by the sample. The measured extensional viscosity flow curve observed here results from the complex interplay between capillary driving force, the accumulated material strain and the instantaneous extension rate; it thus follows a non-linear path through strain/strain–rate/time space. From our data, two general behaviours for all geometrical configurations tested are clear though: first, a mildly extensional thinning viscosity is seen at low strain rates and small strains, and second, a large increase in the extensional viscosity (up to 100 fold) is seen at large strains once a critical Deborah number ($De \sim 1$) has been reached in the thinning filament.

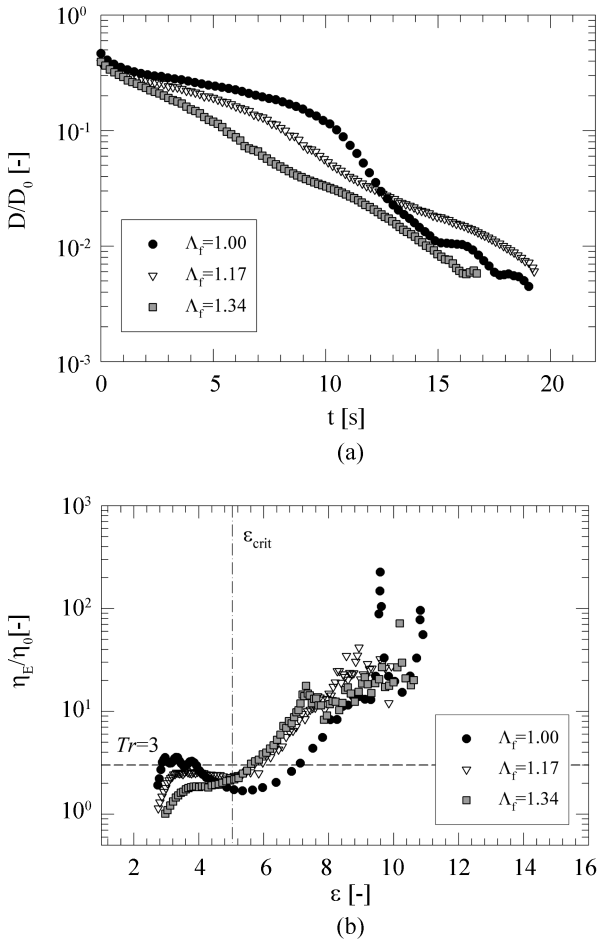

Fig. 4. Filament-thinning profile of CPyCl/NaSal solution with endplate diameter $D_0 = 4.76$ mm and for final aspect ratios given in the legends: (a) instantaneous midplane diameter D as a function of measuring time, (b) Trouton ratio η_E/η_0 as a function of filament strain.

3.3. Varying the sample diameter, D_0

To explore the role of the initial sample dimension and therefore that of the intrinsic Deborah number (see Eq. (8)), experiments with 3.18 mm and 4.76 mm endplates were also conducted (Fig. 4 (a) and 5 (a)). The extensional viscosity as a function of accumulated strain is presented in Fig. 4 (b) and 5 (b). The data exhibit characteristics similar to the experiments with 6 mm endplates, with a constant extensional viscosity regime at low strains, and a thinning extensional viscosity for small initial aspect ratios and the onset of strain-hardening at $\varepsilon \sim 5$.

The data for the 3.18 mm endplates are the least well-defined at small strains ($\varepsilon < 4$) due to the large initial step strain imposed on the sample quickly contracting the filament diameter. Lack of resolution in this regime in experiments with large initial step strains may explain why direct strain-hardening behaviour in CaBER tests was reported for a similar fluid (Bhardwaj *et al.*, 2007a).

The extensional relaxation time was calculated using Eq. (8) from the strain-hardening regime at large strains for all geometrical configurations tested. The ratio of extensional relaxation time to Maxwell relaxation time from small amplitude oscillatory shear tests λ_E/λ_M was plotted against the final aspect ratio imposed by the CaBER test and is shown in Fig. 6. The intrinsic Deborah number De_{int} relates the characteristic viscoelastic timescale of the fluid to the inertiocapillary necking timescale of the thinning filament. Two trends can be observed in the measured relaxation time. First, for increasing final aspect ratio there is an increase in λ_E/λ_M. The second trend is a reduction in experimental variations and a decrease in the aspect ratio dependence for higher values of De_{int}, with $\lambda_E/\lambda_M \approx 1$ for $\Lambda_f > 1.4$ and $De_{int} = 60$. We also plot results from other experiments with wormlike micellar systems similar to the fluids studied in the present work. Bhardwaj *et al.* (2007a) reported the ratio was unity for a final aspect ratio of 1.8. However, Yesilata *et al.* (2006) reported a ratio of relaxation times $\lambda_E/\lambda_M = 1/3$ for three different concentrations of an EHAC

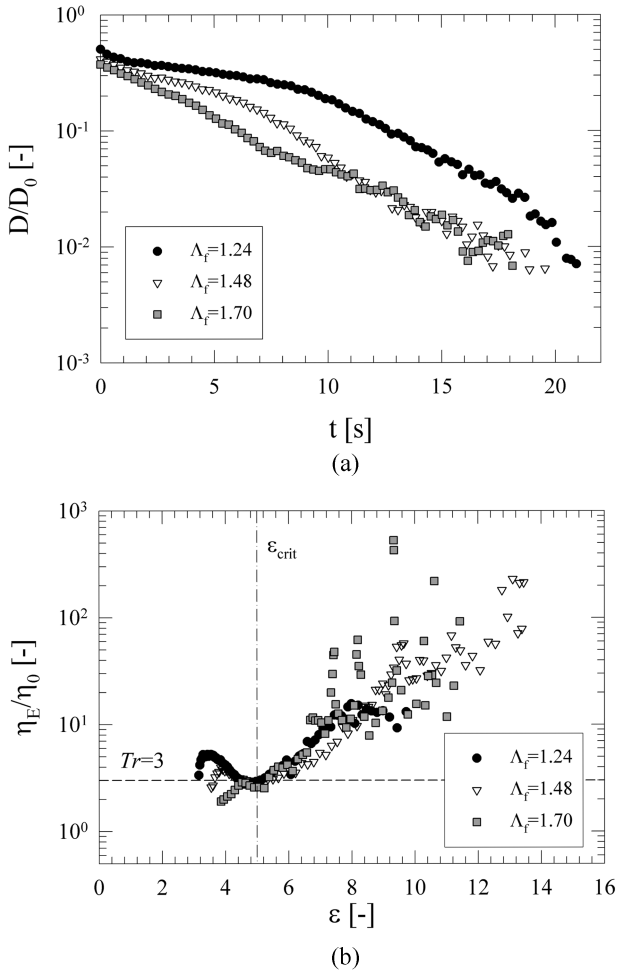

Fig. 5. Filament-thinning profile of CPyCl/NaSal solution with endplate diameter D_0=3.18 mm and varied final aspect ratio: (a) midplane diameter decrease as a function of measuring time, (b) Trouton ratio as a function of filament strain.

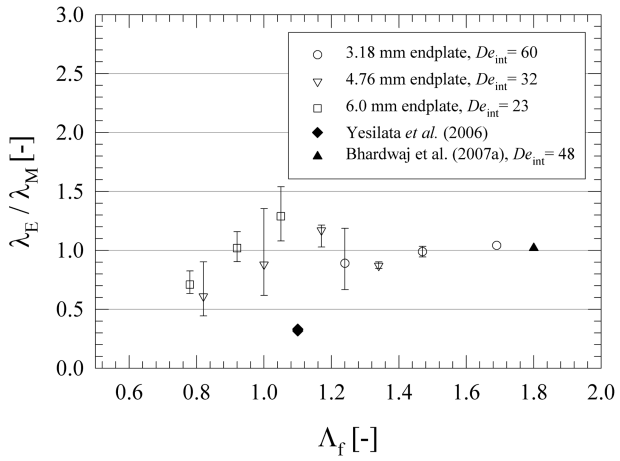

Fig. 6. Variation in the extensional relaxation time λ_E/λ_M of a semidilute CPyCl/NaSal wormlike system as a function of the final aspect ratio $\Lambda_f = h_f/D_0$. The error bars represent the minimum and maximum value in each data set.

system for a fixed final aspect ratio of 1.1. This discrepancy could be due to fundamental properties of this specific wormlike micellar material, but it could be also due to the low aspect ratio stretch. Miller *et al.* (2009) performed a set of experiments for CPyCl/NaSal systems with wider ranges of stretching distances and stretching rates and the extensional relaxation time decreased rapidly to an asymptotic value as the stretching distance or the stretching rate were increased. They could achieve much larger final aspect ratios with a wider range using a larger initial volume, but on the other hand, the stretching rate was somewhat lower than the one used in this study. Therefore it is not possible to compare the two data sets directly, but it is fair to point out that under $\Lambda_f < 2$ for a lower concentration of CPyCl/NaSal system, the extensional relaxation time in their study was close to unity which corresponds to our results.

Capillary breakup experiments with dilute and weakly semidilute polymer solutions have previously shown significant discrepancies between the relaxation times calculated from theoretical models and those measured experimentally (Tirtaatmadja *et al.*, 2006). It has been suggested that these divergences are due to the strong deformation imposed in step extensional strains resulting in significantly different configurations of the suspended polymer chains from those encountered in shearing flow (Clasen *et al.*, 2006; Prabhakar *et al.*, 2006). For the semidilute micellar solution used in the present study, the absence of large, order-of-magnitude differences between the relaxation times measured in shear and elongation (for a wide range of geometrical configurations) suggests that initial conditions do not have a dominant effect on the microstructural relaxation processes at long times, but can give rise to initial regimes of apparent extensional thinning associated with the rearrangement of the liquid bridge. This would be consistent with the scission/recombination processes attributed to entangled wormlike micelles whereby strongly aligned states initially imposed on the micellar network by the step strain deformation are 'forgotten' at long times as the polymer chains break and reassociate.

4. Conclusions

In this study we have explored the extensional behaviour of a CPyCl/NaSal entangled wormlike micellar solution in uniaxial step strain experiments. The role of the geometric configuration has been explored by varying the height of the initial step strain and the radius of the endplates. A complex thinning behaviour is observed for the highly non-linear fluid and regimes of constant extensional viscosity, apparent extensional thinning viscosity and extensional thickening viscosity are seen, depending on the radius of the endplates and the initial strain imposed. As expected for a viscoelastic liquid, for large accumulated

strains $\varepsilon > 5$ the experiments uniformly show an extensional thickening behaviour and large extensional viscosities ($\eta_E/\eta_0 \sim 100$) are measured, in good agreement with previous studies (Bhardwaj *et al.*, 2007a; Yesilata *et al.*, 2006). Small, but systematic variations in the effective viscoelastic relaxation time were observed as the final aspect ratio of the step strain Λ_f and the intrinsic Deborah number De_{int} are varied. As Λ_f was increased, a larger value of λ_E was measured; this effect became less pronounced for larger values of De_{int}. A general trend was observed for increasing De_{int} and increasing Λ_f showing that the measured relaxation times lie closer to the value measured in shear experiments, and have less experimental error.

The relatively mild sensitivity to the initial experimental conditions of the relaxation time measured at large strains is at first surprising for such a highly non-linear material. However, the continual breaking and reforming of the micelles introduces a mechanism whereby the initial deformation history has a reduced impact on the microstructural configuration in the viscoelastic capillary-thinning regime. This picture is consistent with the observed reduction in error in the measured relaxation time and the closer agreement with the value measured in shear for stronger initial deformations. Therefore this suggests that in capillary breakup rheometry the dominant relaxation time is relatively independent of the flow geometry (providing the initial deformation has a sufficiently large aspect ratio Λ_f and intrinsic Deborah number De_{int}). This highlights the utility of CaBER devices for measuring apparent relaxation times and transient extensional viscosities in free-surface flows.

However, for moderate aspect ratios and large strain rates, much remains to be understood about the complex free surface dynamics. Numerical simulations can be used to better understand the complex and coupled interaction between the filament shape, the local deformation rate and accumulated strain in extensional flows of micellar solutions (Cromer *et al.*, 2009). In addition, experiments that are able to provide information on the local microstructural configuration are necessary. In shearing flows, particle image velocimetry (Miller and Rothstein, 2007), dynamic light scattering (Salmon *et al.*, 2003) and nuclear magnetic resonance imaging (Britton and Callaghan, 1997) have been used to understand the local velocity field and guide the development of constitutive models that describe the measured macroscopic stress in terms of the microstructural configuration (Vasquez *et al.*, 2007). Although dynamic light scattering (Chen and Warr, 1997) and flow-induced birefringence (Pathak and Hudson, 2006) experiments have been used to elucidate information on the local micellar structure in steady extension-dominated flows, further detailed investigations of the local strain and stress fields combined with information on the transient evolution of the microstructure are required to fully understand the relationship between applied extensional deformations and the resulting fluid stresses. Microfluidic devices that generate controllable extensional flows hold particular promise here (Pipe and McKinley, 2009).

Acknowledgements

This work was partially supported by the National Research Laboratory Fund (M10300000159) of the Ministry of Science and Technology in Korea. GHM and CJP acknowledge support from NASA under the Microgravity Fluid Sciences program. NJK's exchange visit to the Hatsopoulos Microfluids Laboratory was partially covered by a Class of 1960 Fellowship to GHM.

References

Akers, B. and A. Belmonte, 2006, Impact dynamics of a solid sphere falling into a viscoelastic micellar fluid, *Journal of Non-Newtonian Fluid Mechanics* **135**, 97-108.

Anna, S. L. and G. H. McKinley, 2001, Elasto-capillary-thinning and breakup of model elastic liquids, *Journal of Rheology* **45**, 115-138.

Berret, J.-F., J. Appell and G. Porte, 1993, Linear rheology of entangled wormlike micelles, *Langmuir* **9**, 2851-2854.

Berret, J.-F., G. Porte and J.-P. Decruppe, 1997, Inhomogeneous shear flows of wormlike micelles: A master dynamic phase diagram, *Physical Review E* **55**, 1668-1676.

Berret, J.-F., D. C. Roux and G. Porte, 1994, Isotropic-to-nematic transition in wormlike micelles under shear, *Journal de Physique II* **4**, 1261-1279.

Bhardwaj, A., E. Miller and J. P. Rothstein, 2007a, Filament stretching and capillary breakup extensional rheometry measurements of viscoelastic wormlike micelle solutions, *Journal of Rheology* **51**, 693-719.

Bhardwaj, A., D. Richter, M. Chellamuthu and J. Rothstein, 2007b, The effect of pre-shear on the extensional rheology of wormlike micelle solutions, *Rheologica Acta* **46**, 861-875.

Bhattacharjee, P. K., J. P. Oberhauser, G. H. McKinley, L. G. Leal and T. Sridhar, 2002, Extensional rheometry of entangled solutions, *Macromolecules* **35**, 10131-10148.

Britton, M. M. and P. T. Callaghan, 1997, Two-phase shear band structures at uniform stress, *Physical Review Letters* **78**, 4930.

Britton, M. M., R. W. Mair, R. K. Lambert and P. T. Callaghan, 1999, Transition to shear banding in pipe and couette flow of wormlike micellar solutions, *Journal of Rheology* **43**, 897-909.

Chen, C. M. and G. G. Warr, 1997, Light scattering from wormlike micelles in an elongational field, *Langmuir* **13**, 1374-1376.

Clasen, C., J. P. Plog, W. M. Kulicke, M. Owens, C. Macosko, L. E. Scriven, M. Verani and G. H. McKinley, 2006, How dilute are dilute solutions in extensional flows?, *Journal of Rheology* **50**, 849-881.

Cromer, M. J., L. P. Cook and G. H. McKinley, 2009, Extensional flow of wormlike micellar solutions, *Chemical Engineering Science* **64**, 4588-4596.

Davies, C. J., A. J. Sederman, C. J. Pipe, G. H. McKinley, L. F. Gladden and M. L. Johns, 2010, Rapid measurement of tran-

sient velocity evolution using GERVAIS, *Journal of Magnetic Resonance* **202**, 93-101.

Dhont, J. K. G. and W. J. Briels, 2008, Gradient and vorticity banding, *Rheologica Acta* **47**, 257-281.

Entov, V. M. and E. J. Hinch, 1997, Effect of a spectrum of relaxation times on the capillary-thinning of a filament of elastic liquid, *Journal of Non-Newtonian Fluid Mechanics* **72**, 31-53.

Fischer, P. and H. Rehage, 1997, Non-linear flow properties of viscoelastic surfactant solutions, *Rheologica Acta* **36**, 13-27.

Fischer, P., G. G. Fuller and Z. Lin, 1997, Branched viscoelastic surfactant solutions and their response to elongational flow, *Rheologica Acta* **36**, 632-638.

Grand, C., J. Arrault and M. E. Cates, 1997, Slow transients and metastability in wormlike micelle rheology, *Journal de Physique II* **7**, 1071-1086.

Hu, Y. T. and A. Lips, 2005, Kinetics and mechanism of shear banding in an entangled micellar solution, *Journal of Rheology* **49**, 1001-1027.

Jayaraman, A. and A. Belmonte, 2003, Oscillations of a solid sphere falling through a wormlike micellar fluid, *Physical Review E* **67**, 065301.

Kojic, N., J. Bico, C. Clasen and G. H. McKinley, 2006, *Ex vivo* rheology of spider silk, *The Journal of Experimental Biology* **209**, 4355-4362.

Larson, R. G., 1998, The structure and rheology of complex fluids, Oxford University Press, USA New York.

Lee, J. Y., G. G. Fuller, N. E. Hudson and X.-F. Yuan, 2005, Investigation of shear-banding structure in wormlike micellar solution by point-wise flow-induced birefringence measurements, *Journal of Rheology* **49**, 537-550.

Liang, R. F. and M. R. Mackley, 1994, Rheological characterization of the time and strain dependence for polyisobutylene solutions, *Journal of Non-Newtonian Fluid Mechanics* **52**, 387-405.

McKinley, G. H., 2005, Visco-elasto-capillary-thinning and breakup of complex fluids, *Rheology Reviews* **2005**, 1-48.

McKinley, G. H. and A. Tripathi, 2000, How to extract the newtonian viscosity from capillary breakup measurements in a filament rheometer, *Journal of Rheology* **44**, 653-670.

Miller, E., C. Clasen and J. P. Rothstein, 2009, The effect of step-stretch parameters on capillary breakup extensional rheology (CaBER) measurements, *Rheologica Acta* **48**, 625-639.

Miller, E. and J. P. Rothstein, 2007, Transient evolution of shear-banding wormlike micellar solutions, *Journal of Non-Newtonian Fluid Mechanics* **143**, 22-37.

Nghe, P., G. Degre, P. Tabeling and A. Ajdari, 2008, High shear rheology of shear banding fluids in microchannels, *Applied Physics Letters* **93**, 204102.

Papageorgiou, D. T., 1995a, Analytical description of the breakup of liquid jets, *Journal of Fluid Mechanics* **301**, 109-132.

Papageorgiou, D. T., 1995b, On the breakup of viscous liquid threads, *Physics of Fluids* **7**, 1529-1544.

Pathak, J. A. and S. D. Hudson, 2006, Rheo-optics of equilibrium polymer solutions: Wormlike micelles in elongational flow in a microfluidic cross-slot, *Macromolecules* **39**, 8782-8792.

Petrie, C. J. S., 2006, Extensional viscosity: A critical discussion, *Journal of Non-Newtonian Fluid Mechanics* **137**, 15-23.

Pipe, C. J., T. Majmudar and G. H. McKinley, 2008, High shear rate viscometry, *Rheologica Acta* **47**, 621-642.

Pipe, C. J. and G. H. McKinley, 2009, Microfluidic rheometry, *Mechanical Research Communication* **36**, 110-120.

Pipe, C. J., N. J. Kim, G. H. McKinley, P. A. Vasquez and L. P. Cook, Submitted, Wormlike micellar solutions II: Comparison between experimental data and scission model predictions, *Journal of Rheology*.

Prabhakar, R., J. R. Prakash and T. Sridhar, 2006, Effect of configuration-dependent intramolecular hydrodynamic interaction on elastocapillary-thinning and breakup of filaments of dilute polymer solutions, *Journal of Rheology* **50**, 925-947.

Prud'homme, R. K. and G. G. Warr, 1994, Elongational flow of solutions of rodlike micelles, *Langmuir* **10**, 3419-3426.

Rehage, H. and H. Hoffmann, 1991, Viscoelastic surfactant solutions: Model systems for rheological research, *Molecular Physics* **74**, 933-973.

Rodd, L. E., T. P. Scott, J. J. Cooper-White and G. H. McKinley, 2005, Capillary breakup rheometry of low-viscosity elastic fluids, *Applied Rheology* **15**, 12-27.

Rothstein, J. P., 2003, Transient extensional rheology of wormlike micelle solutions, *Journal of Rheology* **47**, 1227-1247.

Salmon, J.-B., A. Colin, S. Manneville and F. Molino, 2003, Velocity profiles in shear-banding wormlike micelles, *Physical Review Letters* **90**, 228303.

Smolka, L. B. and A. Belmonte, 2003, Drop pinch-off and filament dynamics of wormlike micellar fluids, *Journal of Non-Newtonian Fluid Mechanics* **115**, 1-25.

Sostarecz, M. C. and A. Belmonte, 2004, Beads-on-string phenomena in wormlike micellar fluids, *Physics of Fluids* **16**, L67-L70.

Tirtaatmadja, V., G. H. McKinley and J. J. Cooper-White, 2006, Drop formation and breakup of low viscosity elastic fluids: Effects of molecular weight and concentration, *Physics of Fluids* **18**, 043101-043118.

Turner, M. S. and M. E. Cates, 1991, Linear viscoelasticity of living polymers: A quantitative probe of chemical relaxation times, *Langmuir* **7**, 1590-1594.

Vasquez, P. A., G. H. McKinley and L. P. Cook, 2007, A network scission model for wormlike micellar solutions: I. Model formulation and viscometric flow predictions, *Journal of Non-Newtonian Fluid Mechanics* **144**, 122-139.

Walker, L. M., P. Moldenaers and J.-F. Berret, 1996, Macroscopic response of wormlike micelles to elongational flow, *Langmuir* **12**, 6309-6314.

Yao, M., S. H. Spiegelberg and G. H. McKinley, 2000, Dynamics of weakly strain-hardening fluids in filament stretching devices, *Journal of Non-Newtonian Fluid Mechanics* **89**, 1-43.

Yesilata, B., C. Clasen and G. H. McKinley, 2006, Nonlinear shear and extensional flow dynamics of wormlike surfactant solutions, *Journal of Non-Newtonian Fluid Mechanics* **133**, 73-90.